Effects of monoolein-based cubosome formulations on lipid droplets and mitochondria of HeLa cells

Angela Maria Falchi,*[a] Antonella Rosa,[a] Angela Atzeri,[a] Alessandra Incani,[a] Sandrina Lampis,[b] Valeria Meli,[b] Claudia Caltagirone[b] and Sergio Murgia*[b]

Despite the remarkable development of nanoparticles for different purposes, relatively little is known about their interaction with biological systems and individual cells. Here the effects of two monoolein-based cubosome formulations stabilized by Pluronic F108 and F127 were investigated against HeLa cells. Microscopy analysis on living cells loaded with organelle-specific fluorescent probes was performed to assess the formation of cytoplasmic lipid droplets after nanoparticle treatment. Mitochondrial membrane potential and mitochondrial ROS generation were also investigated in relation to the capability of the accumulated lipids to affect mitochondrial functions. Values of the main cellular unsaturated fatty acids were also measured to assess cell lipid profile modulation. Results from this study show that the uptake of both cubosome formulations induced modification of the cell lipid profile, lipid droplet accumulation, mitochondrial hyperpolarization and mitochondrial ROS generation. These results shed some light on the influence exerted by monoolein-based cubosome formulations on subcellular organelles and their possible adverse effects on cell functions.

Introduction

Monoolein (MO, glycerol monooleate) self-assembles in water, forming a number of nanostructures, including two bicontinuous cubic phases characterized by a different space group: the *Ia3d*, and the *Pn3m*.[1] These amazing liquid crystalline nanostructures are composed of a curved bilayer whose three-dimensional folding originates two disconnected, continuous water channels.[2,3] They were ubiquitously found in Nature, and several studies were dedicated to shed some light on their role in the cell machinery.[4–6] Since MO-based bicontinuous cubic phases are nanostructures that can suitably host hydrophobic molecules with biological relevance, they were extensively investigated in the past for their possible applications in the pharmaceutical field.[7–9] Remarkably, cubic phases can be formulated as nanoparticle dispersions, known as cubosomes, typically stabilized in water using amphiphilic polymers having long polyethylene oxide (PEO) chains, such as Pluronics or polysorbate 80.[10–12] These liquid crystalline nanoparticles are often proposed to be suitable drug delivery nanocarriers

and, recently, their possible application as theranostic nanomedicine was discussed in several papers.[13–15] However, little information about *in vitro* cellular interactions and toxicity of monoolein-based cubosomes has been reported so far, and the lack of shared protocols precludes straightforward comparisons between these investigations. For example, focusing on monoolein-based formulations exposed to adherent cells, to the best of our knowledge only six papers (two from our group, not including the present) have discussed the cytotoxicity of pristine cubosomes (*i.e.*, not decorated with targeting agents or loaded with drugs/imaging agents).[13,16–20] In all these cases, experiments were performed using different cell lines, at different incubation times, and with formulations having different compositions (basically, they were prepared using a different monoolein/Pluronic ratio, sometimes using different types of Pluronic). It is worth noting that several papers have reported on the haemolytic properties of monoolein-based cubosome formulations tested on mouse blood,[18,21] indicating 20 μg mL^{-1} of monoolein as the maximum tolerable concentration.[20] However, another recent investigation conducted on human and porcine plasma has disputed these results, attributing to the same formulation a very low haemolytic activity.[22] We have previously shown no toxic effects of monoolein-based nanoparticles (liposomes and cubosomes) at short times against HeLa cells and 3T3 fibroblasts[16,23] based on an 80% viability threshold.

[a]*Department of Biomedical Sciences, University of Cagliari, 09042 Monserrato, CA, Italy. E-mail: amfalchi@unica.it; Fax: +39 070 6754003; Tel: +39 070 6754055*
[b]*Department of Chemical and Geological Sciences, University of Cagliari, 09042 Monserrato, CA, Italy. E-mail: murgias@unica.it; Fax: +39 070 6754003; Tel: +39 070 6754388*

All cell types have been found to readily take up the lipids present in culture media and sequester them into lipid droplets (LDs). LDs are cytoplasmic organelles that consist of a hydrophobic core of neutral lipids (such as triglycerides and cholesterol esters) encased by a phospholipid monolayer harboring a set of enzymes and regulatory proteins that catalyze the highly metabolically controlled synthesis and mobilization of fat stores.[24] LDs, found in almost all cells under physiological or pathological conditions, are heterogeneous not only in size but also in the lipid content and the composition of their protein coat.[25] The most widely accepted model for LD formation hypothesizes that they arise in the endoplasmic reticulum (ER) through the accumulation of neutral lipid at specific sites between the leaflets of the phospholipid bilayer (ER budding model).[24] Dynamical interactions between LDs and organelles other than ER, including mitochondria and peroxisomes, have been suggested to facilitate the exchange of proteins and lipids in cells, while interactions between the ER and mitochondria are crucial for processes such as lipid synthesis, storage and transport as well as mitochondrial functions (calcium homeostasis and apoptosis).[26,27]

In the present study, we used organelle-specific dyes to explore the changes occurring in lipid droplets and mitochondria of living HeLa cells when exposed to treatment with monoolein-based cubosomes stabilized by Pluronic F108 or Pluronic F127. Analyses were carried out to examine lipid droplet content, mitochondria membrane potential, reactive oxygen species (ROS), and cellular lipid profile at 4 and 24 h after nanoparticle treatment. Our results demonstrate that the uptake of both cubosome formulations induces a modification in the cellular lipid profile, accumulation of lipid droplets associated with a significant dysfunction of mitochondria,

including mitochondrial hyperpolarization and mitochondrial ROS generation.

Results and discussion

Cubosome characterization

Colloidal dispersions of a bicontinuous cubic phase (cubosomes) were prepared by dispersing *via* sonication melted monoolein (MO) either in a Pluronic F108 (PF108) or in a Pluronic F127 (PF127) aqueous solution. These nanoparticle formulations were then characterized for particle size and morphology, as well as for their inner structure. The cryo-TEM images of MO-based PF127 and PF108 stabilized cubosomes (MO/PF127 and MO/PF108) are shown in Fig. 1A and B. These images show various nanoparticles revealing the regular alternation of bright spots (water channels) and dark matrix (lipid bilayer) classically observed in the presence of a cubic arrangement of the interface, along with the vesicular material that typically co-exists with the cubosomes in these kinds of formulations.[16] On the basis of repeated observations, the samples under investigation *via* cryo-TEM were found to be a dispersion of cubosomes having diameter in the range of 100–200 nm, in striking agreement with DLS analysis (Table 1). SAXS definitely confirmed the inner cubic structure of both cubosome formulations. As reported in Table 1, the diffraction patterns showed the Bragg peaks of the bicontinuous cubic double diamond and primitive phases (with space groups *Pn3m* and *Im3m*, respectively, see also Fig. 1C and D). It deserves noticing that the simultaneous presence of these two phases has already been described for cubosome formulations having composition similar to those investigated here,[28] and their occur-
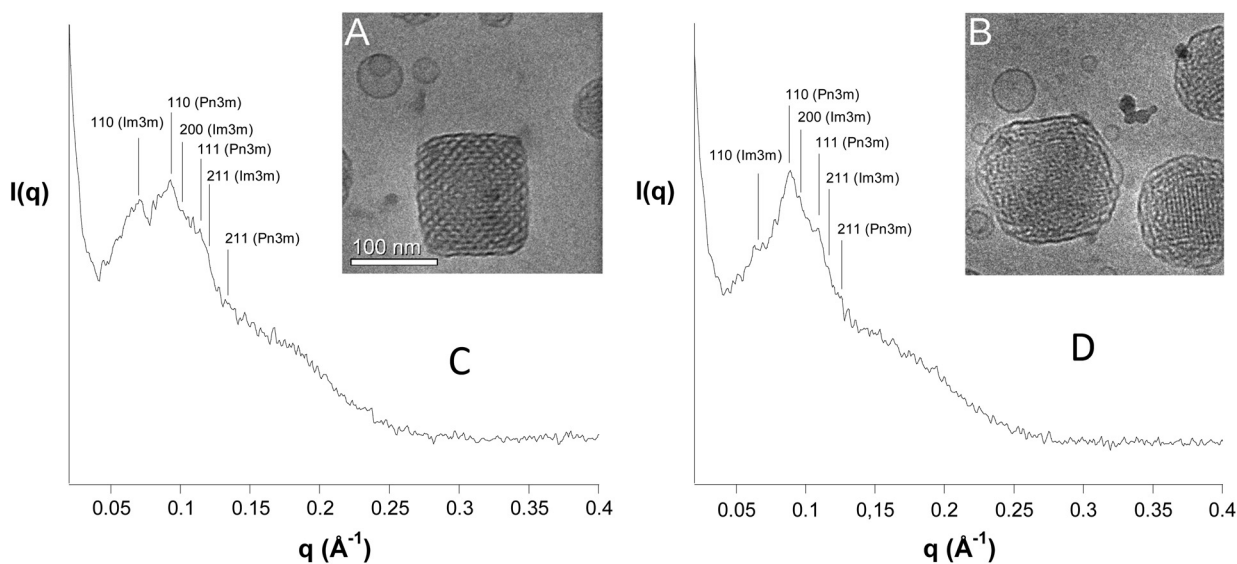
Fig. 1 Cryo-TEM images of MO-based cubosomes stabilized by PF127 (A) and PF108 (B). *I(q)* *vs*. *q* data obtained by SAXS of the cubosome formulation stabilized by PF127 (C) and PF108 (D). The Miller indices are reported on top of the corresponding Bragg peaks along with the indication of the space group.

Table 1 Space group, lattice parameter (a), mean diameter (D_{av}), polydispersion index (PDI), and ζ-potential of the cubosome nanoparticles stabilized with either PF108 or PF127

Cubosome stabilizers	Space group	a (Å)	D_{av} (nm)	PDI	ζ-Potential (mV)
PF108	Pn3m	101 ± 4	133 ± 1	0.11	−28 ± 2
	Im3m	137 ± 4			
PF127	Pn3m	98 ± 3	136 ± 2	0.14	−19 ± 1
	Im3m	136 ± 6			

rence is explained with the non-uniform partition of the Pluronic. Indeed, during the dispersion process the dispersant preferentially localizes at the cubosome surface, originating Pluronic-depleted regions characterized by double diamond symmetry.[29]

Accumulation of lipids in the lipid droplets

Several studies have shown LD accumulation after treatment with free fatty acids[30] or associated with oxidative stress induced by nanoparticle treatment.[31,32] Indeed, after the internalization in the cells, unsaturated fatty acids such as oleic acid (OA) can be either esterified and stored as neutral lipids inside LDs or become part of the cellular membranes or, after activation to fatty acyl-CoAs, oxidized in mitochondria for energy production.[30] Here, to investigate LD accumulation, HeLa cells were treated with cubosome formulations (5 μL in 1 mL of medium) at 4 and 24 h and, after nanoparticle washout, co-loaded with Nile Red (NR) and Hoechst probes, to stain LDs and the nucleus, respectively.

In untreated control cells the number of small LDs, detected as punctuated green fluorescent cytoplasmic structures, was very different from cell to cell. Upon short exposure to cubosomes, the number of lipid droplets dispersed throughout the cytoplasm and their size increased in a remarkable way and droplets appeared larger and more numerous in all cells (Fig. 2A), suggesting that LD accumulation results from the synthesis of neutral lipids from nanoparticle-derived monoolein.

When compared to untreated control cells, an increase in the IOD (Integrated Optical Density) per cell of 7.9 ($p < 0.001$)- and 3.1 ($p < 0.001$)-fold was estimated for, respectively, MO/PF127 and MO/PF108, indicating a statistically significantly increased production of LDs (Fig. 2B). Subsequently, HeLa cells were grown in the presence of MO dissolved in DMSO and Pluronic aqueous solutions (administered at the same concentrations as MO and Pluronics present in the cubosome formulations) and OA (18:1 n-9) (used as the positive control at the non-cytotoxic concentration of 100 μM in DMSO). At short times, MO and OA treatments caused 1.3 ($p < 0.05$)- and 2.8 ($p < 0.001$)-fold increase, respectively, in IOD per cell in comparison with untreated cells, whereas Pluronic solutions showed the same IOD per cell as the control (Fig. 2B). At longer exposure time (24 h), differently from MO- and OA-treated cells where the IOD did not change, the IOD of

MO/PF127 and MO/PF108-treated cells increased by 25.6 ($p < 0.001$)- and 31.5-fold ($p < 0.001$), respectively. Because of the huge cubosome uptake, cells appeared to be full of lipids inside the cytoplasm with many large droplets aggregated in several clusters resembling grapes (Fig. 2A and B).

While the LD formation induced by long-chain unsaturated fatty acids such as OA is a well-known phenomenon, data reported here proved that LD formation also occurs upon MO and MO-based cubosome treatment. Compared with MO-treated cells, statistically significantly increased production of lipid droplets was detected after cubosome exposure, thus suggesting a strong internalization ability of both MO-based cubosome formulations. Since the amount of MO administered was exactly the same, the differences could be ascribed to different uptake mechanisms. Indeed, while nanoparticles can be transported into the cells *via* endocytosis, the fatty acid uptake across the lipid bilayer of the plasma membrane was proposed to proceed by diffusion or through membrane-associated proteins (acting as fatty acid transporters).[33,34] Remarkably, statistically significant differences ($p < 0.001$) between the two cubosome formulations were observed in the IOD only at short time treatments.

Modification of the lipid cell profile

The same MO/PF108 and MO/PF127 cubosome formulations and MO, OA, and Pluronic solutions previously described were then tested to assess their effects on the lipid composition of HeLa cells. After 4 and 24 h of incubation, the cell lipid fraction was extracted and the variations in the levels of unsaturated fatty acids and cholesterol were analyzed with respect to untreated control cells. The unsaturated fatty acid composition (expressed as μg per plate) and the chromatographic profile of HeLa control cells obtained by HPLC are shown in Fig. 3. The cell content of the most abundant unsaturated fatty acids was detected as follows: 78.19, 19.87, 6.38, 4.89, 3.11, and 3.05 μg per plate for 18:1 isomers (OA and 18:1 n-7), 16:1 n-7, arachidonic acid (20:4 n-6), docosahexaenoic acid (DHA, 22:6 n-3), eicosapentaenoic acid (EPA 20:5 n-3), and 18:2 n-6, respectively; minor amounts were measured for 18:3 n-3, 20:3, and 22:4 n-6. The incubation of HeLa cells with PF108 or PF127 solution did not induce changes in unsaturated fatty acid levels, with treated cells showing a profile similar to that of control cells at both incubation times (data at 4 h are shown in Fig. 3A).

Fig. 4 shows the values of the most abundant unsaturated fatty acids 16:1 n-7, 20:4 n-6, DHA, OA, and cholesterol (expressed as % of the control) measured in HeLa cells after 4 (Fig. 4A) and 24 h (Fig. 4B) of incubation in the presence of cubosomes, MO, and OA. The incubation of cells at 4 h treatment with the compounds induced a significant increase in the cell level of OA, which reached values approximately 3, 3, 2, and 2 times higher than that of the control cells in MO/PF108, MO/PF127, MO and OA treated cells, respectively. Treatments were not associated with changes in the levels of all the other unsaturated fatty acids. Experiments performed at 24 h of incubation time revealed a further increase of the OA levels
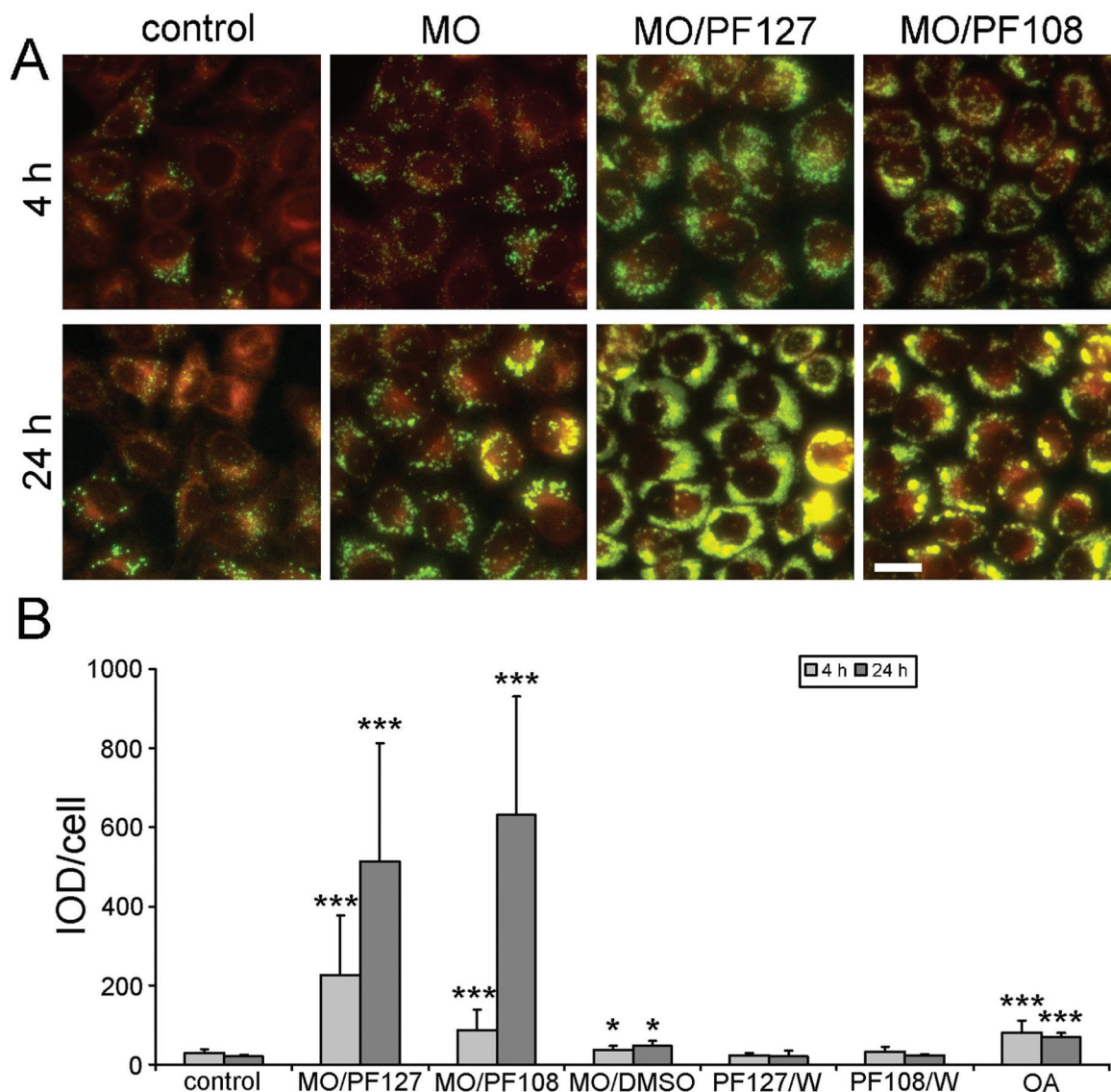
Fig. 2 Lipid droplet accumulation induced in HeLa cells by cubosome treatment. (A) Representative composite color images of HeLa cells exposed to the monoolein (MO), MO/PF127 and MO/PF108 cubosomes at 4 and 24 h of incubation time. Membranes (red) and lipid droplets (green) were stained with Nile Red (colocalization in yellow). Scale bar = 20 μm. (B) Results of the lipid droplet formation at 4 and 24 h of incubation time. Oleic acid (OA) was used as the positive control at the non-cytotoxic concentration of 100 μM. Data are expressed as mean ± SD from four independent experiments. Statistically significant differences are indicated by * ($p < 0.05$), *** ($p < 0.001$) by t-test vs. untreated-control cells.

(5 times higher than the control) in cells treated with cubosome formulations, while levels of all the other unsaturated fatty acids remained substantially unaltered with respect to the control. Remarkably, the levels of OA recorded in MO and OA treated cells were very similar to those observed at 4 h-treated HeLa cells. This result parallels the finding discussed in the previous paragraph concerning the lipid droplet accumulation and, similarly, can be reconciled taking into account the different uptake mechanisms. Using HPLC, the total cholesterol level was measured in control cells as the mean content of 72.52 ± 0.55 μg per plate. Fig. 4 also shows the values of cholesterol measured in the control and 4 and 24 h-treated

HeLa cells. The different treatments did not seem to affect the level of cholesterol.

Mitochondrial membrane potential

Mitochondria play a central role in normal cell functions such as energy supply and in cell death by inducing apoptosis. Changes in the mitochondrial membrane potential (mitoMP) represent one of the adaptation processes to a variety of environmental factors that regulate the increased energy demands, cell growth and differentiation, or cellular stress. In mitochondria, mitoMP is produced by the electron transport chain as it pumps H^+ ions into the membrane space,
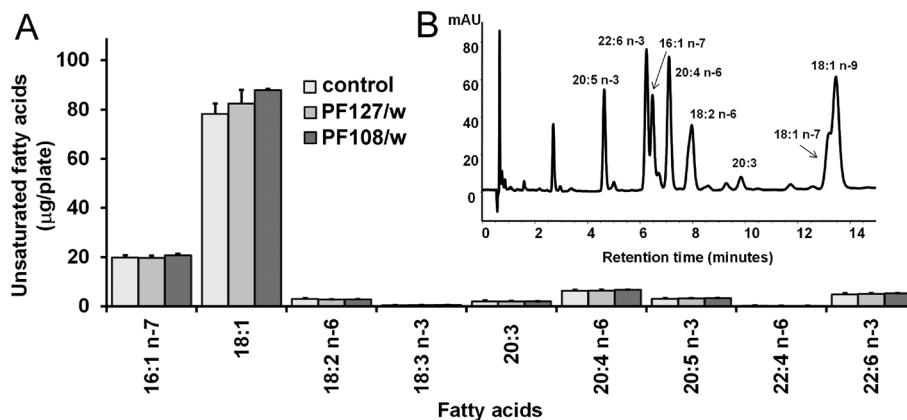
Fig. 3 Fatty acid composition and chromatographic profile of HeLa cells. Values of the unsaturated fatty acids (16:1 n-7, 18:1, 18.2 n-6, 18:3 n-3, 20:3, 20:4 n-6, 20:5 n-3, 22:4 n-6, 22:6 n-3, expressed as μg per plate) measured in control cells and after 4 h of incubation in the presence of PF127 and PF108 solutions (A) and the corresponding HPLC chromatographic profile of the control HeLa cells (B). Data are expressed as mean ± SD from four independent experiments (involving duplicate analyses for each sample).
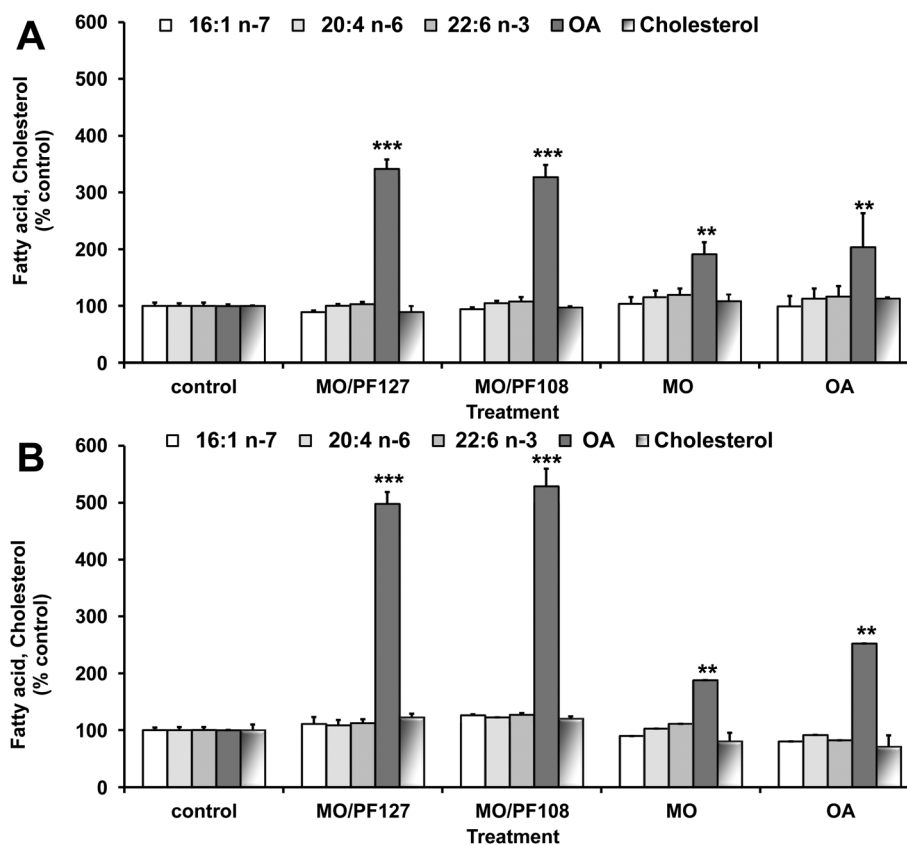

Fig. 4 Lipid profile modulation in cubosome-treated cells. The values of the main unsaturated fatty acids, 16:1 n-7, 18:1 (OA), 20:4 n-6, 22:6 n-3, and cholesterol (expressed as % of the control) measured in HeLa control cells and after 4 (A) and 24 h (B) of incubation in the presence of MO/PF127 and MO/PF108 cubosomes, MO, and OA (used as the positive control). Data are expressed as mean ± SD from four independent experiments (involving duplicate analyses for each sample). Statistically significant differences, using one-way analysis of variation (one-way ANOVA) and the Bonferroni post test (GraphPad INSTAT software, San Diego, CA), are indicated by ** ($p < 0.01$), *** ($p < 0.001$) vs. untreated-control cells.

thus creating an electrochemical proton gradient which drives ATP synthesis. Variations of mitoMP are usually measured in living cells with the cationic fluorescent dye TMRM, which accumulates in the mitochondrial matrix driven by the voltage gradient across the inner mitochondrial membrane. Using the TMRM probe, control cells showed morphologically
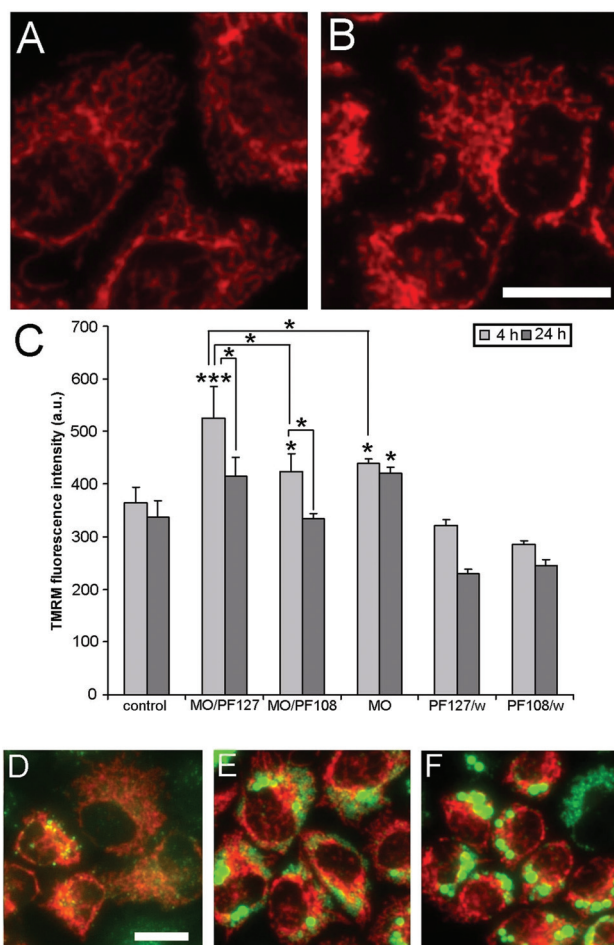
Fig. 5 Effect of cubosome treatment on mitochondrial membrane potential and mitochondrial network appearance. (A, B) Representative images of the control (A) and short-term cubosome-treated (B) cells stained with the mitochondria-specific dye TMRM. Scale bar = 20 μm. (C) Analysis of mitochondrial membrane potential (mitoMP) evaluated by TMRM fluorescence intensity (arbitrary units) in the control and treated cells. Data are expressed as the mean ± SD from four independent experiments. Statistically significant differences are indicated by *($p <$ 0.05), ***($p < 0.001$) by t-test $vs.$ untreated-control cells and among differently treated cells. (D–F) Representative composite color images of HeLa cells, co-loaded with TMRM (red) and Bodipy 493/503 (green), after 24 h of incubation time with MO (D), MO/PF127 (E) and MO/PF108 (F) cubosomes. Scale bar = 10 μm.

smooth and variously stained mitochondrial filaments (Fig. 5A).

Following short term incubation of HeLa cells with both cubosome formulations and MO, a significant hyperpolarization of the mitochondrial membrane potential was observed as compared with untreated-control cells (Fig. 5B and C). Moreover, MO/PF127-treated cells showed a larger mitoMP ($p < 0.05$) than MO/PF108- and MO-treated cells. In contrast, analysis of mitoMP in cells treated with Pluronic solutions showed the same mitoMP as the control. At long time treatment, differently from MO-treated cells, a significant decrease of mitoMP ($p < 0.05$) was detected in both cubosome-treated cells.

On co-loading cells with TMRM and Bodipy 493/503, it was observed that, in cubosome-treated cells, the cytoplasmic distribution of mitochondria (the so-called mitochondrial networking) was considerably modified, and unlike MO-treated cells where the mitochondrial network appeared to be regular (Fig. 5D), clusters of mitochondria were confined in various areas of the cytoplasm and excluded by the large droplets (Fig. 5E and F). Therefore, the loss of mitoMP associated with altered mitochondrial morphology could suggest that, at long time treatment, mitochondrial dysfunction arises from lipid accumulation.[35]
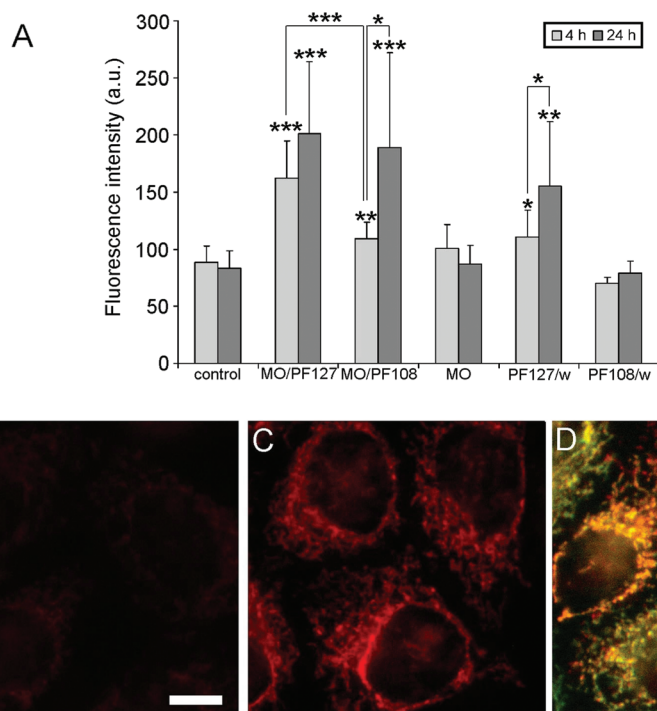
Mitochondrial ROS generation

The mitochondrion is the major free radical-producing compartment of the cell, representing, at the same time, an important target for the reactive oxygen species (ROS) action. Mitochondrial ROS production usually occurs during electron transport along the respiratory chain complexes, and same pathophysiological conditions can increase mitochondrial ROS generation such as an enhancement of the mitochondrial membrane potential.[36] To specifically investigate the effect of nanoparticles on mitochondrial ROS generation, control and treated cells were loaded with the mitochondrial superoxide indicator MitoROS Red in combination with the mitochondria-specific probe MitoTracker Green with the aim of verifying the mitochondrial origin of ROS and correlating mtROS with changes in the mitochondrial morphology. A significant and progressively increased ROS production was detected in cells treated with both types of cubosomes as compared with the control and MO-treated cells (Fig. 6A–C). ROS production increased by 1.3 ($p < 0.01$)- and 1.9-fold ($p < 0.001$) at short term treatment and by 2.3- and 2.4-fold ($p < 0.001$) at long time exposure to, respectively, MO/PF108 and MO/PF127 cubosomes. The mitochondrial origin of ROS was confirmed by their co-localization with MitoTracker Green. It is worth mentioning that, in cells with high mtROS levels, mitochondria appeared fragmented (Fig. 6D), suggesting involvement of the mitochondrial permeability transition pore (mPTP) and the inner membrane anion channel (IMAC) in maintaining healthy mitochondria homeostasis.[37]

Analysis of the mtROS level in HeLa cells treated with Pluronic solutions showed different results (Fig. 6A). Whereas in PF108 solution-treated cells, mtROS production was not dissimilar from the control and MO-treated cells, cells treated with a PF127 solution showed a significant mtROS increase at both 4 h and 24 h treatment. This effect is in agreement with that reported in a previous study where Pluronic P85 co-localized with mitochondria and caused mitochondria impairment accompanied by ROS production.[38]

Nuclear staining and externalization of phosphatidylserine

LD and mitoMP evaluation was performed on cubosome-treated cells with no signs of morphological damage and/or chromatin condensation (Fig. 7A). Chromatin condensation was determined by nuclear staining with Hoechst 33258. After 4 h cubosome treatment along with healthy cells, we detected

Fig. 6 Mitochondrial ROS generation. (A) Analysis of mitochondrial ROS evaluated by MitoSOX fluorescence intensity (arbitrary units) in untreated-control and treated cells. Data are expressed as mean ± SD from four independent experiments. Statistically significant differences are indicated by *($p < 0.05$), **($p < 0.01$), ***($p < 0.001$) by t-test $vs.$ untreated-control cells and among differently treated cells. (B, C) Representative images of MitoSOX Red fluorescence in untreated (B) and short-term cubosome-treated (C) cells. (D) Composite color image of cubosome-treated cells co-loaded with MitoSOX Red (red) and MitoTracker Green (green), co-localization in yellow-orange. Scale bar = 10 μm.
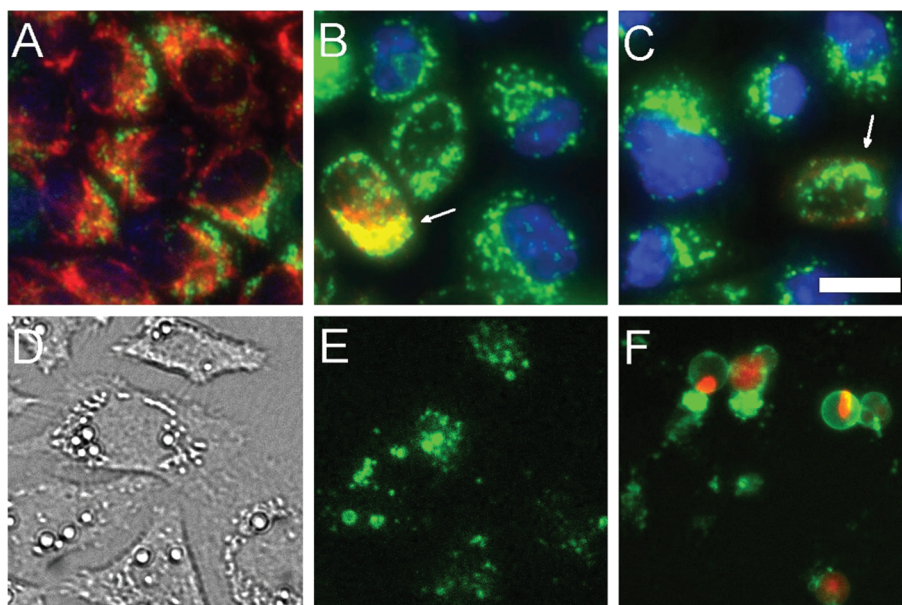
Fig. 7 Cells undergoing apoptosis with chromatin condensation and externalized PS. (A–C) Merged color images of cubosome-treated cells co-loaded with TMRM (red), Bodipy 493/503 (green) and Hoechst 33258 (HOE, blue) probes. (A) Healthy cells showing polarized mitochondria, lipid droplet accumulation and no signs of chromatin condensation. (B, C) Round cells, full of cytoplasmic lipids, showing chromatin condensation (HOE-positive) and depolarized mitochondria (TMRM-negative). Arrows indicate some round cells showing still polarized mitochondria. (D–F) Phase contrast (D) and relative fluorescence image (E) of cells showing distinct round domains positive for FITC-Annexin V with nuclei negative for propidium iodide (PI). (F) Apoptotic cells positive for FITC-Annexin V and PI. Scale bars = 10 μm.

the presence of clusters of round cells (still attached at the dish) with the cytoplasm full of lipids, showing condensed nuclei and low or completely missing TMRM fluorescence, indicating mitochondrial depolarization (Fig. 7B and C). To verify whether these round cells were undergoing apoptosis, untreated control and cubosome-treated cells were co-stained with FITC-conjugated Annexin V and propidium iodide (PI). As untreated-control cells were largely negative for externalized phosphatidylserine (PS) and nuclear condensation, in cells treated with cubosomes we were able to observe and distinguish differently labeled cells: (a) healthy cells (~80%), negative for both Annexin-FITC and PI (Fig. 7A); (b) cells undergoing apoptosis (~15%), with exposed PS Annexin positive and PI negative (Fig. 7D and E); (c) apoptotic cells (~5%), positive for both Annexin-FITC and PI (Fig. 7F). This result showed the slight impact of the cubosomes on the cells and, at the same time, confirmed that lipid loading might induce apoptosis in cells.

MTT assay

The effects of cubosome formulations, MO, PF127 and PF108 solutions were evaluated against HeLa cells at 4 and 24 h according to the MTT assay, which is sensitive to mitochondrial activity and is used to evaluate cell apoptosis and cell division inhibition. The MTT value of non-treated control cells was set to 100% and the values of treated cells were expressed as a percent of the control. As shown in Fig. 8, a slight decrease of MTT reduction was observed with both cubosome formulations (but also with MO and Pluronic solutions) in the first 4 h of incubation time. Remarkably, at long term exposure (24 h), the absorbance of cubosome-treated cells increased and was not different from control cells, whereas treatment with MO and both Pluronic solutions showed the same decrease as MTT reduction at short time. This unexpected

result may be due to variation in the redox status of the cells and/or mitochondrial membrane hyperpolarization and/or interference of the MTT reaction with the large amount of LDs in the cell cytoplasm. Indeed various lines of evidence suggest that MTT formazan deposits accumulate in the lipid droplets.[39,40] According to MTT results further supported by fluorescence analysis, HeLa cells appeared healthy beside mitochondrial dysfunction and lipid droplet accumulation, suggesting no relevant toxic effect of cubosome treatment at these incubation times and this concentration.

Conclusion

Here, the effects caused by two different cubosome formulations on HeLa cells were compared. The formulations were prepared using the same building block (monoolein), but were stabilized by two different Pluronics. By employing multiple labeling with organelle-specific dyes, we provide a helpful procedure to investigate nanoparticle–cell interactions. Results evidenced that both cubosome formulations influenced the cell behavior and, particularly, organelles such as lipid droplets and mitochondria. In long time experiments the differences between the two cubosome formulations were levelled out, but significant differences were observed at short time treatments.
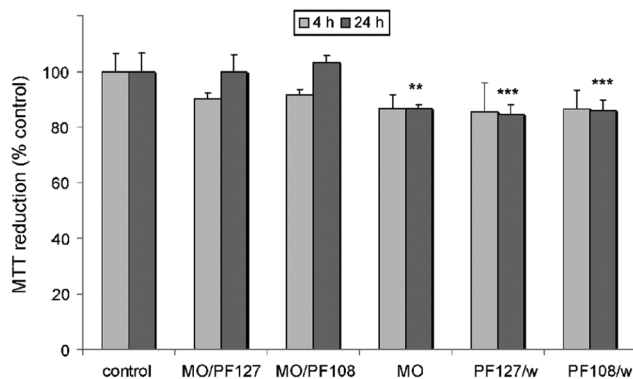
Physicochemical investigations demonstrated that, from a morphological point of view, two almost indistinguishable formulations were compared. Moreover, the lipid profile confirmed that the same amount of formulation was taken up by the cells. Therefore, the detected differences can be entirely ascribed to the different Pluronic used to stabilize the cubosome formulations, and could be explained in terms of the different hydrophobicity of these block copolymers, as exemplified by their Hydrophilic Lipophilic Balance values (HLB equal to 22 and 27 for PF127 and PF108, respectively).[41] Results concerning the Pluronic solutions evidenced different mitochondrial ROS production depending on the dispersant used, reinforcing this hypothesis. The MTT test proved the low toxicity of these formulations against HeLa cells at the concentration used in this investigation (165 µg mL^{-1} of monoolein). This finding agrees with others previously reported on the same cellular line.[17]

Taking into consideration the close advent on the market of various nanotechnologically based products, we strongly believe that the presented results may be useful to understand the impact of cubosome formulations in biological tissues and their possible hazardous nature.

Fig. 8 Results of the MTT assay of HeLa cells exposed to treatment with cubosomes, monoolein and Pluronic solutions. The MTT value of non-treated control cells was set to 100% and the values of treated cells were expressed as a percent of the control. Data are expressed as the mean ± SD from three independent experiments (involving triplicate analyses for each sample). Statistically significant differences are indicated by **($p < 0.01$) and ***($p < 0.001$) vs. untreated-control cells by t-test.

Experimental

Cubosome preparation

Cubosomes were prepared by dispersing the appropriate amount of melted monoolein (MO) in an aqueous solution of Pluronic (F108 or F127) using an ultrasonic processor UP100H

by Dr Hielscher, cycle 0.9, amplitude 90%, for 10 minutes. The sample volume was 4 mL with 96.4 wt% of water, 3.3 wt% of MO and 0.3 wt% of Pluronic (F108 or F127). MO (RYLO MG 19 PHARMA, glycerol monooleate, 98.1 wt%) was kindly provided by Danisco A/S, DK-7200, Grinsted, Denmark. Pluronic F108 (PEO_{132}–PPO_{50}–PEO_{132}) and Pluronic F127 (PEO_{100}–PPO_{65}–PEO_{100}) were purchased from Sigma-Aldrich. Distilled water passed through a Milli-Q water purification system (Millipore) was used to prepare the samples.

Cryogenic-transmission electron microscopy (cryo-TEM)

Vitrified specimens were prepared in a controlled environment vitrification system (CEVS) at 25 °C and 100% relative humidity. A drop of the sample was placed on a perforated carbon film-coated copper grid, blotted with filter paper, and plunged into liquid ethane at its freezing point. The vitrified specimens were transferred to a 626 Gatan cryo-holder, and observed at 120 kV acceleration voltage in a FEI Tecnai T12 G2 transmission electron microscope at about −175 °C in the low-dose imaging mode to minimize electron-beam radiation-damage. Images were digitally recorded with a Gatan US1000 high-resolution CCD camera.

Small-angle X-ray scattering (SAXS) experiments

Small-angle X-ray scattering was recorded with an S3-MICRO SWAXS camera system (HECUS X-ray Systems, Graz, Austria). Cu K_α radiation of wavelength 1.542 Å was provided by a GeniX X-ray generator, operating at 50 kV and 1 mA. A 1D-PSD-50 M system (HECUS X-ray Systems, Graz, Austria) containing 1024 channels of width 54.0 μm was used for the detection of scattered X-rays in the small-angle region. The working q-range ($Å^{-1}$) was $0.003 \leq q \leq 0.6$, where $q = 4\pi \sin(\theta)\lambda^{-1}$ is the scattering wave vector. Thin-walled 2 mm glass capillaries were used. The lattice parameter a of the cubic phase was determined using the relation $a = d(h^2 + k^2 + l^2)^{1/2}$ from linear fits of the plots of $1/d$ versus $(h^2 + k^2 + l^2)^{1/2}$, where $d = 2\pi/q$ and h, k, and l are the Miller indices.

Dynamic light scattering (DLS)

Particle size and ζ-potential determinations of the nanoparticles were performed with a ZetaSizer Nano ZS (Malvern Instruments, Malvern, UK) at a temperature of 25 ± 0.1 °C. Samples were backscattered by a 4 mW He–Ne laser (operating at a wavelength of 633 nm) at an angle of 173°. Diluted samples (1 : 50) were housed in disposable polystyrene cuvettes of 1 cm optical path length with water as the solvent. At least 2 independent samples were taken, each of which was measured 3–5 times. The width of the DLS hydrodynamic diameter distribution is indicated by PDI (polydispersion index).

Cell culture and treatments

The human cervical carcinoma cell line HeLa (ATCC collection), chosen as model cancer cells, was grown in phenol red-free Dulbecco's modified Eagle's medium (DMEM, Invitrogen, USA) with high glucose, supplemented with 10% (v/v) fetal bovine serum, penicillin (100 U mL^{-1}) and streptomycin (100

μg mL^{-1}) (Invitrogen) in a 5% CO_2 incubator at 37 °C. Cells were seeded in 35 mm dishes and experiments were carried out two days after seeding when cells had reached 90% confluency. MO-based cubosomes were added to the cells at a concentration of 1 : 200 (5 μL in 1 mL of fresh medium) and incubated at 37 °C for 4 and 24 h. Treatments were also performed with oleic acid (OA) in DMSO (100 μM), MO in DMSO (463 μM) and Pluronic F108 and F127 aqueous solutions (205 μM and 238 μM, respectively) equimolar respectively with the lipid and surfactant present in the cubosome formulations. OA and MO stock solutions in DMSO were 1000-fold concentrated to not exceed the 0.1% concentration of vehicle in the medium. The same concentration of vehicle was added to control cells when required by experimental design. For live cell imaging, fresh serum-free medium was used to remove the extracellular particle suspension. Then, cells were loaded with fluorescent probes and, after the incubation time, the latter were washed before the imaging session.

Fluorescence microscopy

Cells were stained with the following probes: 300 nM Nile Red (NR) (9-diethylamino-5H-benzo[a]phenoxazine-5-one) for 15 min; 25 nM tetramethylrhodamine methyl ester perchlorate (TMRM) for 30 min; 5 μM MitoSox Red for 10 min; 100 nM MitoTracker Green FM (MitoTracker) for 30 min; 38 μM Bodipy 493/503 for 30 min; 650 nM Hoechst 33258 for 30 min. NR was from Fluka (Buchs, SG, Switzerland); TMRM, MitoTracker Green, MitoSox Red and Bodipy 493/503 were from Molecular Probes (Eugene, OR, USA); Hoechst from Sigma-Aldrich (St. Louis, MO, USA). Microscopy observations were made using a Zeiss (Axioskop) upright fluorescence microscope (Zeiss, Oberkochen, Germany) equipped with 10×, 20× and 40×/0.75 NA water immersion objectives and a HBO 50 W L-2 mercury lamp (Osram, Berlin, Germany). Twelve-bit-deep images were acquired with a monochrome cooled CCD camera (QICAM, Qimaging, Canada) with variable exposure. For the observation of TMRM and MitoSOX, filters were: ex 546 ± 6 nm, em 620 ± 60 nm. For MitoTracker Green, Bodipy 493/503 and Annexin V-FITC, filters were: ex 470 ± 20 nm, em 535 ± 40 nm. For Hoechst 33258, filters were: ex 360 ± 20 nm, em 460 ± 25 nm. For Nile Red, filters were: ex 470 ± 20 nm, em 535 ± 40 nm for nonpolar lipids; ex 546 ± 6 nm, em 620 ± 60 nm for total lipids.

Lipid droplet quantification

Fluorescent-based detection of the lipid droplet number, volume and cellular distribution is usually achieved in live cells with NR and Bodipy 493/503. NR is an ideal probe for the detection of lipids, as it exhibits high affinity, specificity and sensitivity to the degree of hydrophobicity of lipids. The latter feature results in a shift of the emission spectrum from red to green in the presence of polar and non-polar lipids respectively.[42] For this reason, on staining living cells with NR, the cytoplasmic membranes are stained in red whereas neutral lipids of LDs are stained in green. Fluorescence images of NR-stained cells were acquired at 10× under a fluorescence micro-

scope. Measurements concerned the amount of LD content that was evaluated by the fluorescence intensity of NR-green emission. IOD (Integrated Optical Density) per cell was calculated using Image ProPlus software. Alternatively, LDs were stained with Bodipy 493/503. This nonpolar dye for neutral lipid staining was used when cells were co-loaded with TMRM or MitoSOX Red for simultaneous observations of LDs with mitochondria or mitochondrial ROS, respectively.

Detection of mitochondrial membrane potential and mitochondria-derived ROS

TMRM is a red potential-sensitive probe that is concentrated inside mitochondria by their negative membrane potential. MitoTracker Green FM is a green selective dye that localizes to the lipid environment of the mitochondria. MitoSOX Red is a live-cell permeant fluorogenic probe that is selectively targeted to the mitochondria of live cells. Once in the mitochondria, MitoSOX Red is oxidized by superoxide anions and exhibits red fluorescence. In order to analyze the mitochondrial membrane potential (mitoMP) and the mitochondrial production of superoxide anions (mtROS), cells were incubated with TMRM or MitoSOX and, after removal of the probes from the medium, images of living cells were captured under a fluorescence microscope. The fluorescence intensities of TMRM and MitoSOX were assumed to be a conventional estimate of mitoMP and mtROS concentrations, respectively. Using Image ProPlus software, the fluorescence intensity of TMRM and MitoSOX was measured around the perinuclear area where mitochondria are densely packed. Mitochondrial fragmentation was morphologically assessed.

Imaging

Fluorescence intensity measurements, made on a single cell basis, were performed with Image ProPlus software (Media Cybernetics, Silver Springs, MD) in the following way: cells were seeded in 35 mm dishes and, after nanoparticle treatment, loaded with fluorescent probes. Ten randomly selected fields were acquired from each dish using a 10× objective. Data of the fluorescence intensity of NR, TMRM or MitoSOX were expressed as the mean ± standard deviation (SD) of four independent experiments. Statistical evaluations were done by Student's t-test. The differences were considered to be significant at $p < 0.05$ (*), $p < 0.01$ (**) and $p < 0.001$ (***).

Nuclear and Annexin V-FITC staining

Cells were co-loaded with the DNA fluorochrome Hoechst 33258 together with all dyes. This probe is a water-soluble nuclear dye commonly used to distinguish apoptotic nuclei (characterized by nuclear condensation of chromatin and/or nuclear fragmentation) from healthy ones. To visualize the externalized phosphatidylserine (PS) as an early apoptosis marker, treated cells were incubated with FITC-conjugated Annexin V and propidium iodide (PI) for 10 min at room temperature according to the Instruction Manual for the kit (Annexin V-FITC Apoptosis detection kit, Sigma-Aldrich).[43] FITC-conjugated Annexin V and PI were detected as green and

red fluorescence, respectively. Fluorescence images were acquired at 10× and viable and non-viable cells were counted in each field (5 fields per well) using Image ProPlus. Results are expressed as the percent ratio of damaged *versus* total number of cells.

Extraction and analyses of cell lipid components

Total lipids were extracted from HeLa cell pellets using the Folch procedure.[44] The $CHCl_3$ fraction, containing the lipids, from each cell sample was dried down and dissolved in EtOH. Separation of cholesterol and unsaturated fatty acids was obtained by mild saponification.[45] The hexane phase containing the unsaponifiable fraction (cholesterol) was collected and the solvent was evaporated. A portion of the dried residue, dissolved in MeOH, was injected into the high-performance liquid chromatography (HPLC) system. The hexane phase (saponifiable fraction) with fatty acids, dissolved in CH_3CN with 0.14% CH_3COOH (v/v), was injected into the HPLC system. The recovery of fatty acids and cholesterol during the saponification was calculated using an external standard mixture prepared by dissolving 1 mg of triolein, trilinolein, and cholesterol in EtOH and processed as samples. All solvent evaporation was performed under vacuum. Analyses of cholesterol and unsaturated fatty acids were carried out with an Agilent Technologies 1100 HPLC (Agilent Technologies, Palo Alto, CA) equipped with a diode array detector as previously described.[45] Identification of lipid components was made using standard compounds and the conventional UV spectra, generated using the Agilent OpenLAB CDS Chemstation C.01.04. Calibration curves of all of the compounds were constructed using standards and were found to be linear, with correlation coefficients >0.995. Cholesterol, triolein, trilinolein, standards of fatty acids, high-purity solvents, and Desferal were purchased from Sigma-Aldrich. Data are expressed as mean ± SD from four independent experiments (involving duplicate analyses for each sample). Statistically significant differences, using one-way analysis of variation (one-way ANOVA) and the Bonferroni post test (GraphPad INSTAT software, San Diego, CA), are indicated by *($p < 0.05$), **($p < 0.01$) and ***($p < 0.001$).

MTT assay

HeLa cells were seeded in 24-well plates (3×10^4 cells per well), cultured overnight and then treated with the cubosomes, MO and Pluronic solutions for 4 and 24 h at the same concentrations as those described in the "Cell culture and treatments" section. After removal of the extracellular particle suspension with fresh serum-free medium, cells were incubated with MTT (3(4,5-dimethylthiazolyl-2)-2,5-diphenyltetrazolium bromide) (0.5 mg mL^{-1}) for 2 h at 37 °C, and then lysed with DMSO. Absorbance was measured at 570 nm using an Infinite auto 200 microplate reader (Infinite 200, Tecan, Austria). Results are shown as percent of cell viability in comparison with non-treated control cells. Data are expressed as mean ± SD from three independent experiments (involving triplicate analyses for each sample). Statistical evaluations

were done by Student's t-test. The differences were considered to be significant at $p < 0.05$ (*), $p < 0.01$ (**) and $p < 0.001$ (***).

Conflict of interest

The authors declare that they have no conflict of interest.

Funding sources

Acknowledgements

References

1 S. T. Hyde, *J. Phys. Chem.*, 1989, **93**, 1458.
2 K. Larsson, *J. Phys. Chem.*, 1989, **93**, 7304.
3 S. Hyde, S. Andersson, K. Larsson, Z. Blum, T. Landh, S. Lidin and B. W. Ninham, *The Language of Shape*, Elsevier, Amsterdam, 1997.
4 Z. A. Almsherqi, S. D. Kohlwein and Y. Deng, *J. Cell Biol.*, 2006, **173**, 839.
5 Z. A. Almsherqi, T. Landh, S. D. Kohlwein and Y. Deng, *Int. Rev. Cell Mol. Biol.*, 2009, **274**, 275.
6 S. Murgia, S. Lampis, P. Zucca, E. Sanjust and M. Monduzzi, *J. Am. Chem. Soc.*, 2010, **132**, 16176.
7 J. Shah, Y. Sadhale and D. M. Chilukuri, *Adv. Drug Delivery Rev.*, 2001, **47**, 229.
8 F. Caboi, G. S. Amico, P. Pitzalis, M. Monduzzi, T. Nylander and K. Larsson, *Chem. Phys. Lipids*, 2001, **109**, 47.
9 S. Murgia, F. Caboi and M. Monduzzi, *Chem. Phys. Lipids*, 2001, **110**, 11.
10 T. Landh, *J. Phys. Chem.*, 1994, **98**, 8453.
11 X. Mulet, B. J. Boyd and C. J. Drummond, *J. Colloid Interface Sci.*, 2013, **393**, 1.
12 F. Tiberg, M. Johnsson, J. Barauskas and A. Norlin, *J. Nanosci. Nanotechnol.*, 2006, **6**, 3017.
13 B. W. Muir, D. P. Acharya, D. F. Kennedy, X. Mulet, R. A. Evans, S. M. Pereira, K. L. Wark, B. J. Boyd, T.-H. Nguyen, T. M. Hinton, L. J. Waddington, N. Kirby, D. K. Wright, H. X. Wang, G. F. Egan and B. A. Moffat, *Biomaterials*, 2012, **33**, 2723.
14 C. Caltagirone, A. M. Falchi, S. Lampis, V. Lippolis, V. Meli, M. Monduzzi, L. Prodi, J. Schmidt, M. Sgarzi, Y. Talmon, R. Bizzarri and S. Murgia, *Langmuir*, 2014, **3**, 6228.
15 S. Murgia, S. Bonacchi, A. M. Falchi, S. Lampis, V. Lippolis, V. Meli, M. Monduzzi, L. Prodi, J. Schmidt, Y. Talmon and C. Caltagirone, *Langmuir*, 2013, **29**, 6673.
16 S. Murgia, A. M. Falchi, M. Mano, S. Lampis, R. Angius, A. M. Carnerup, J. Schmidt, G. Diaz, M. Giacca, Y. Talmon and M. Monduzzi, *J. Phys. Chem. B*, 2010, **114**, 3518.
17 S. Deshpande, E. Venugopal, S. Ramagiri, J. R. Bellare, G. Kumaraswamy and N. Singh, *ACS Appl. Mater. Interfaces*, 2014, **6**, 17126.
18 T. M. Hinton, F. Grusche, D. Acharya, R. Shukla, V. Bansal, L. J. Waddington, P. Monaghan and B. W. Muir, *Toxicol. Res.*, 2014, **3**, 11.
19 S. Murgia, A. M. Falchi, V. Meli, K. Schillén, V. Lippolis, M. Monduzzi, A. Rosa, J. Schmidt, Y. Talmon, R. Bizzarri and C. Caltagirone, *Colloids Surf., B*, 2015, **129**, 87.
20 N. Tran, X. Mulet, A. M. Hawley, T. M. Hinton, S. T. Mudie, B. W. Muir, E. C. Giakoumatos, L. J. Waddington, N. M. Kirby and C. J. Drummond, *RSC Adv.*, 2015, **5**, 26785.
21 J. Barauskas, C. Cervin, M. Jankunec, M. Špandyreva, K. Ribokaitė, F. Tiberg and M. Johnsson, *Int. J. Pharm.*, 2010, **391**, 284.
22 J. C. Bode, J. Kuntsche, S. S. Funari and H. Bunjes, *Int. J. Pharm.*, 2013, **448**, 87.
23 M. Carboni, A. M. Falchi, S. Lampis, C. Sinico, M. L. Manca, J. Schmidt, Y. Talmon, S. Murgia and M. Monduzzi, *Adv. Healthcare Mater.*, 2013, **2**, 692.
24 S. O. Olofsson, P. Bostrom, L. Andersson, M. Rutberg, J. Perman and J. Boren, *Biochim. Biophys. Acta*, 2009, **1791**, 448.
25 M. Digel, R. Ehehalt and J. Fullekrug, *FEBS Lett.*, 2010, **584**, 2168.
26 M. Beller, K. Thiel, P. J. Thul and H. Jackle, *FEBS Lett.*, 2010, **584**, 2176.
27 J. E. Vance, *Biochim. Biophys. Acta*, 2014, **1841**, 595.
28 M. Nakano, A. Sugita, H. Matsuoka and T. Handa, *Langmuir*, 2001, **17**, 3917.
29 M. Nakano, T. Teshigawara, A. Sugita, W. Leesajakul, A. Taniguchi, T. Kamo, H. Matsuoka and T. Handa, *Langmuir*, 2002, **18**, 9283.
30 Y. Fujimoto, J. Onoduka, K. J. Homma, S. Yamaguchi, M. Mori, Y. Higashi, M. Makita, T. Kinoshita, J. Noda, H. Itabe and T. Takanoa, *Biol. Pharm. Bull.*, 2006, **29**, 2174.
31 A. Khatchadourian and D. Maysinger, *Mol. Pharm.*, 2009, **6**, 1125.
32 D. Maysinger, *Org. Biomol. Chem.*, 2007, **5**, 2335.
33 H. Hillaireau and P. Couvreur, *Cell. Mol. Life Sci.*, 2009, **66**, 2873.
34 X. Su and A. A. Abumrad, *Trends Endocrinol. Metab.*, 2009, **20**, 72.
35 C. L. Gao, C. Zhu, Y. P. Zhao, X. H. Chen, C. B. Ji, C. M. Zhang, J. G. Zhu, Z. K. Xia, M. L. Tong and X. R. Guo, *Mol. Cell. Endocrinol.*, 2010, **320**, 25.
36 L. Formentini, M. Sanchez-Arago, L. Sanchez-Cenizo and J. M. Cuezva, *Mol. Cell*, 2012, **45**, 731.
37 D. B. Zorov, M. Juhaszova and S. J. Sollot, *Physiol. Rev.*, 2014, **94**, 909.

38 D. Y. Alakhova, N. Y. Rapoport, E. V. Batrakova, A. A. Timoshin, S. Li, D. Nicholls, V. Y. Alakhov and A. V. Kabanov, *J. Controlled Release*, 2010, **142**, 89.

39 G. Diaz, M. Melis, A. Musinu, M. Pliludu, M. Piras and A. M. Falchi, *Eur. J. Histochem.*, 2007, **51**, 213.

40 J. C. Stockert, A. Blazquez-Castro, M. Canete and R. W. Horobin, *Acta Histochem.*, 2012, **114**, 785.

41 M. Y. Kozlov, N. S. Melik-Nubarov, E. V. Batrakova and A. V. Kabanov, *Macromolecules*, 2000, **33**, 3305.

42 P. Greenspan, E. P. Mayer and S. D. Fowler, *J. Cell Biol.*, 1985, **100**, 965.

43 S. Y. Hwang, S. H. Cho, B. H. Lee, Y. J. Song and E. K. Lee, *Apoptosis*, 2011, **16**, 1068.

44 J. Folch, M. Lees and G. H. Sloane Stanley, *J. Biol. Chem.*, 1957, **226**, 497.

45 A. Rosa, A. Rescigno, A. Piras, A. Atzeri, P. Scano, S. Porcedda, P. Zucca and M. A. Dessi, *Food Chem. Toxicol.*, 2012, **50**, 3799.